AIAA-2002-0261

An Adjoint Method for the Calculation of Remote Sensitivities in Supersonic Flow

Siva K. Nadarajah*, Antony Jameson† and Juan Alonso‡
Department of Aeronautics and Astronautics
Stanford University
Stanford, California 94305 U.S.A.

Abstract

This paper presents an adjoint method for the calculation of remote sensitivities in supersonic flow. The goal is to develop a set of discrete adjoint equations and their corresponding boundary conditions in order to quantify the influence of geometry modifications on the pressure distribution at an arbitrary location within the domain of interest. First, this paper presents the complete formulation and discretization of the discrete adjoint equations. The special treatment of the adjoint boundary condition to obtain remote sensitivities is also discussed. Secondly, we present results that demonstrate the application of the theory to a three-dimensional remote inverse design problem using a low sweep biconvex wing and a highly swept blunt leading edge wing. Lastly, we present results that establish the added benefit of using an objective function that contains the sum of the remote inverse and drag minimization cost functions.

Introduction

The objective of this work is to develop the necessary methods and tools to facilitate the design of low sonic boom aircraft that can fly supersonically over land with negligible environmental impact. Traditional methods to reduce the sonic boom signature were targeted towards reducing aircraft weight, increasing lift-to-drag ratio, improving the specific fuel consumption, etc. Seebass and Argrow[1] revisited sonic boom minimization and provided a detailed study of sonic boom theory and figure of merits for the level of sonic booms.

In this paper, the control theory approach is used to develop an automatic aerodynamic optimization method to reduce the sonic boom signature. The mathematical theory for the control of systems governed by partial differential equations, as developed by Lions et al.,[5] significantly lowers the computational cost and is clearly an improvement over classical finite-difference methods. Recently, with the help of faster computing resources, automatic aerodynamic optimization has been revisited by Jameson et al.[7–11]

In the control theory approach the gradient is calculated indirectly by solving an adjoint equation. The total cost to obtain these gradients is independent of the number of design variables. The additional overhead of solving the adjoint equation is negligible since the overall cost to obtain the gradients is low. If N design variables are desired, then the finite difference method would require N flow calculations to obtain the gradient. However, with the adjoint method the cost of obtaining the gradient amounts to one flow solution and one adjoint solution. The adjoint problem is a linear PDE of lower complexity than the flow solver. This method was first applied to transonic flow by Jameson.[7] In the last six years the method has been successfully used to optimize complex three dimensional configurations including wing-fuselage combinations and complete aircraft by Jameson et al.,[12,13] Vassberg et al.,[14] Reuther et al.,[15,16] and Burgreen et al.[17]

The adjoint equation can be derived using either a continuous or discrete approach. The discrete adjoint approach applies control theory directly to the discrete field equations. The discrete adjoint equation is then derived by collecting together all the terms multiplied by the variation $\delta w_{i,j}$ of the discrete flow variables. A detailed comparison of the continuous and discrete adjoint approaches was conducted by Nadarajah et al.[18,19] Extensive work on the discrete adjoint method has also been con-

*PhD Candidate, Student Member AIAA
†Thomas V. Jones Professor of Engineering, Stanford University, AIAA Fellow
‡Assistant Professor, Stanford University

tributed by Shubin et al.[22] ,Beux et al.[23] ,Elliot et al.[24] ,Anderson et al.[25] ,Iollo et al.[26] ,and Ta'saan et al.[27]

Sonic Boom Minimization

Traditional adjoint implementations were aimed at reducing a cost function computed from the pressure distribution on the surface that is being modified. In this case, however, we would like to obtain sensitivity derivatives of pressure distributions that are not collocated at the points where the geometry is being modified. This type of sensitivity calculation has not been attempted before and will be necessary for the sonic boom minimization problem. In order to include the tailoring of the ground pressure signatures, it becomes necessary to compute sensitivity derivatives of the sonic boom signature with respect to a large number of design variables that affect the shape of the airfoil or aircraft.

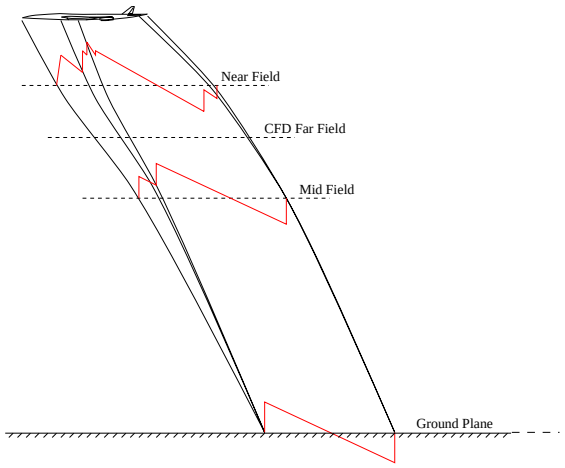

Figure 1: Schematic of Sonic Boom Minimization

For typical cruise altitudes required for aircraft efficiency, the distance from the source of the acoustic disturbance to the ground is typically greater than 50,000 ft. A reasonably accurate propagation of the pressure signature can only be obtained with small computational mesh spacings that would render the analysis of the problem intractable for even the largest parallel computers. An approach that has been used successfully in the past is the use of near to far field extrapolation of pressure signatures based on principles of geometrical acoustics and nonlinear wave propagation. These methods are based on the solutions of simple ordinary differential equations for the propagation of the near field pressure signature to the ground.

Figure 1 is a schematic of the sonic boom minimization problem. 'CFD Far Field' indicates the far field boundary of the mesh. At a pre-specified distance below the aircraft and still within the CFD mesh, the location of a near field plane can be seen. This plane is the effective interface between the CFD solution and the wave propagation program. At the near field plane, the flow solution w_o is represented using a number of parameters, M, which can be taken as the number of mesh points on which the pressure waveform has a value different from the free stream.

The lower portion of the domain between the CFD near field and the ground plane is where the pressure signature propagation method will be active. Given the conditions, w_o, the propagation altitude, and the altitude dependent atmospheric properties $\rho(z), p(z), T(z)$, the propagation method produces a flow solution at the ground plane we are interested in, which can be used to determine any of a variety of measures of sonic boom impact such as overpressures, rise time, impulse, etc. This work focuses on controlling the near field signature which will be the input to the propagation program. The issue of choosing a near field signature to produce a desired ground signature is addressed in an accompanying paper by Alonso et al.[20]

Through the support of the DARPA QSP Program (Grant No: MDA972-01-2-0003), advanced algorithms for the design and optimization of quiet supersonic platforms have been developed at Stanford in the last one year. Our experience has indicated that large reductions in the ground peak pressure cannot be achieved with minor shape modifications of the baseline configuration. Alternative design methods such as genetic algorithms have been used in a multi-level design environment to get in the neighborhood of the optimum design before switching over to a gradient-based method to refine the design. Promising results have been achieved by using genetic algorithms in a linear method environment. Once the ground peak pressure is at a desired level, then nonlinear methods using control theory were developed in order to meet several goals: first, to verify if not improve the results of the linear based method; second, to improve the design by using the remote inverse adjoint method; lastly, to allow the introduction of more objective functions to improve the final design.

The adjoint approach to aerodynamic shape optimization has been under development at Stanford for the past several years through the generous sup-

port of the AFOSR under grant number AF F49620-98-1-022. In this paper, a proof of concept of the remote inverse problem will be demonstrated in three dimensional supersonic flow. The possibility that the adjoint method could be adapted to solve the remote inverse problem was first demonstrated by Nadarajah et al.[21] for a two dimensional internal flow problem.

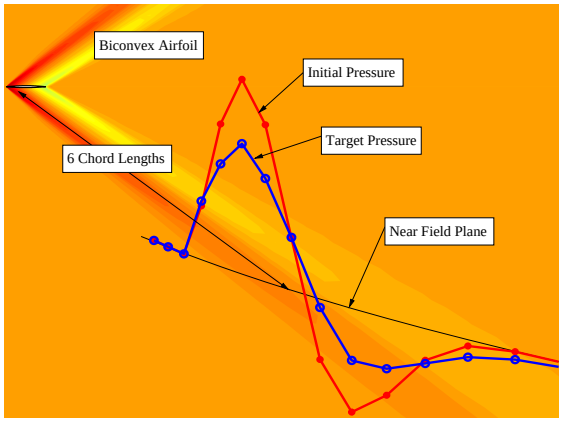

Figure 2: Pressure Contour and Near Field Pressure Distribution for Biconvex Airfoil at Mach 1.5

Figure 2 illustrates the pressure contour and near field pressure distribution for a biconvex airfoil at Mach 1.5. In this two dimensional example, the near field is approximately 6 chord lengths from the airfoil surface. The discrete adjoint boundary condition developed to calculate remote sensitivities is applied along this location. The following sections will clearly demonstrate this method.

The Remote Inverse Design Problem using Control Theory

The aerodynamic properties that define the cost function are functions of the flow-field variables, w, and the physical location of the boundary, which may be represented by the function S.

Suppose that the performance is measured by a cost function

$$I = \varpi_1 \int_{\mathcal{B}_W} \mathcal{M}\left(w, S\right) d\mathcal{B}_\xi + \varpi_2 \int_{\mathcal{B}_{NF}} \mathcal{N}\left(w, S\right) d\mathcal{B}_\xi,$$

containing both wall boundary ($\mathcal{B}_W$) and near field boundary ($\mathcal{B}_{NF}$) contributions, where $d\mathcal{B}_\xi$ includes the surface and near field elements in the computational domain, while ϖ_1 and ϖ_2 are the weighting coefficients. The coordinates ξ_i that describe the fixed computational domain are chosen so that each boundary conforms to a constant value of one of these coordinates. In general, $\mathcal{M}$ and $\mathcal{N}$ will depend on both the flow variables w and the metrics S defining the computational space.

The design problem is now treated as a control problem where the boundary shape represents the control function, which is chosen to minimize I subject to the constraints defined by the flow equations. A shape change produces a variation in the flow solution δw and the metrics δS which in turn produce a variation in the cost function

$$\delta I = \varpi_1 \int_{\mathcal{B}_W} \delta\mathcal{M}(w, S)\, d\mathcal{B}_\xi + \varpi_2 \int_{\mathcal{B}_{NF}} \delta\mathcal{N}(w, S)\, d\mathcal{B}_\xi, \tag{1}$$

with

$$\begin{aligned} \delta\mathcal{M} &= \left[\mathcal{M}_w\right]_I \delta w + \delta\mathcal{M}_{II}, \\ \delta\mathcal{N} &= \left[\mathcal{N}_w\right]_I \delta w + \delta\mathcal{N}_{II}, \end{aligned} \tag{2}$$

where we use the subscripts I and II to distinguish between the contributions associated with the variation of the flow solution δw and those associated with the metric variations δS. Thus $\left[\mathcal{M}_w\right]_I$ and $\left[\mathcal{N}_w\right]_I$ represent $\frac{\partial\mathcal{M}}{\partial w}$ and $\frac{\partial\mathcal{N}}{\partial w}$ with the metrics fixed, while $\delta\mathcal{M}_{II}$ and $\delta\mathcal{N}_{II}$ represent the contribution of the metric variations δS to $\delta\mathcal{M}$ and $\delta\mathcal{N}$ with the flow solution fixed.

The weak form of the Euler equations for steady flow is

$$\int_{\mathcal{D}} \frac{\partial\psi^T}{\partial\xi_i} \delta F_i d\mathcal{D} = \int_{\mathcal{B}} n_i \psi^T \delta F_i d\mathcal{B}.$$

where the test vector ψ is an arbitrary differentiable function and n_i is the outward normal at the boundary. If a differentiable solution w is obtained to this equation, then it can be integrated by parts to give

$$\int_{\mathcal{D}} \psi^T \frac{\partial}{\partial\xi_i} \delta F_i d\mathcal{D} = 0. \tag{4}$$

Since this is true for any ψ, the differential form can be recovered. Here δF_i can be split into contributions associated with δw and δS using a similar notation

$$\delta F_i = \left[F_{i_w}\right]_I \delta w + \delta F_{i\,II} \quad \text{where,} \quad \left[F_{i_w}\right]_I = S_{ij} \frac{\partial f_j}{\partial w}.$$

The domain can then be split into two parts as shown in Figure 3. First, the near field domain ($\mathcal{D}_1$) whose boundaries are the wing surface and the near field boundary plane. Second, the far field domain ($\mathcal{D}_2$) which borders the near field domain along the

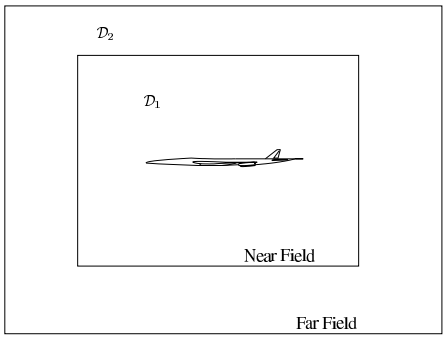

Figure 3: Near Field and Far Field Domains

near field boundary plane and the far field boundary.

$$\int_{\mathcal{D}_1} \psi^T \frac{\partial}{\partial \xi_i} \delta F_i d\mathcal{D}_\xi + \int_{\mathcal{D}_2} \psi^T \frac{\partial}{\partial \xi_i} \delta F_i d\mathcal{D}_\xi = 0.$$

This may be integrated by parts to give

$$\begin{aligned} &\int_{\mathcal{B}_W} n_i \psi^T \delta F_i d\mathcal{B}_\xi - \int_{\mathcal{D}_1} \frac{\partial \psi^T}{\partial \xi_i} \delta F_i d\mathcal{D}_\xi \quad (5) \\ &+ \int_{\mathcal{B}_{NF}} n_i \left(\psi^+ - \psi^-\right)^T \delta F_i d\mathcal{B}_\xi \\ &- \int_{\mathcal{D}_2} \frac{\partial \psi^T}{\partial \xi_i} \delta F_i d\mathcal{D}_\xi = 0. \end{aligned}$$

where ψ^+ and ψ^- are the values of ψ above and below the boundary. Since the left hand expression equals zero, it may be subtracted from the variation in the cost function (1) to give

$$\begin{aligned} \delta I &= \int_{\mathcal{B}_W} \left[\varpi_1 \delta \mathcal{M} - n_i \psi^T \delta F_i\right] d\mathcal{B}_\xi \\ &+ \int_{\mathcal{B}_{NF}} \left[\varpi_2 \delta \mathcal{N} - n_i \left(\psi^+ - \psi^-\right)^T \delta F_i\right] d\mathcal{B}_\xi \\ &+ \int_{\mathcal{D}_1} \frac{\partial \psi^T}{\partial \xi_i} \delta F_i d\mathcal{D}_\xi + \int_{\mathcal{D}_2} \frac{\partial \psi^T}{\partial \xi_i} \delta F_i d\mathcal{D}_\xi. \quad (6) \end{aligned}$$

Now, since ψ is an arbitrary differentiable function, it may be chosen in such a way that δI no longer depends explicitly on the variation of the state vector δw. The gradient of the cost function can then be evaluated directly from the metric variations without having to re-compute the variation δw resulting from the perturbation of each design variable.

Comparing equations (2) and (5), the variation δw may be eliminated from (6) by equating all field terms with subscript "I" to produce a differential adjoint system governing ψ

$$\left[\frac{\partial \psi^T}{\partial \xi_i} \left[F_{iw}\right]_I\right]_{\mathcal{D}_1+\mathcal{D}_2} = 0 \quad \text{in } \mathcal{D}. \quad (7)$$

The corresponding wall and near field adjoint boundary conditions are produced by equating the subscript "I" boundary terms in equation (6) to produce

$$n_i \psi^T \left[F_{iw}\right]_I = \varpi_1 \mathcal{M}_w \quad \text{on } \mathcal{B}_W. \quad (8)$$

$$n_i \left(\psi^+ - \psi^-\right)^T \left[F_{iw}\right]_I = \varpi_2 \mathcal{N}_w \quad \text{on } \mathcal{B}_{NF}. \quad (9)$$

The remaining terms from equation (6) then yield a simplified expression for the variation of the cost function which defines the gradient

$$\begin{aligned} \delta I &= \int_{\mathcal{B}_W} \left\{\varpi_1 \delta \mathcal{M}_{II} - n_i \psi^T \left[\delta F_i\right]_{II}\right\} d\mathcal{B}_\xi \\ &+ \int_{\mathcal{B}_{NF}} \left\{\varpi_2 \delta \mathcal{N}_{II} - n_i \left(\psi^+ - \psi^-\right)^T \left[\delta F_i\right]_{II}\right\} d\mathcal{B}_\xi \\ &+ \int_{\mathcal{D}_1+\mathcal{D}_2} \left\{\frac{\partial \psi^T}{\partial \xi_i} \left[\delta F_i\right]_{II}\right\} d\mathcal{D}_\xi. \quad (10) \end{aligned}$$

The details of the formula for the gradient depend on the way in which the boundary shape is parameterized as a function of the design variables and the way in which the mesh is deformed as the boundary is modified.

The boundary conditions satisfied by the flow equations restrict the form of the left hand side of the adjoint boundary conditions (8) and (9). Consequently, the boundary contribution to the cost functions $\mathcal{M}$ and $\mathcal{N}$ cannot be specified arbitrarily. Instead, it must be chosen from the class of functions which allow cancellation of all terms containing δw in the boundary integral of equation (6).

Design Using the Euler Equations

The adjoint formulation in the previous section was derived using the continuous adjoint approach. In this paper, the discrete adjoint approach was chosen.

The discrete adjoint equation is obtained by applying control theory directly to the set of discrete field equations. The resulting equation depends on the type of scheme used to discretize the flow equations. The work in this paper uses a cell centered multigrid scheme with upwind-biased blended first-and-third-order fluxes for artificial dissipation, local time stepping, and implicit residual smoothing. A full discretization of the equation would involve discretizing every term that is a function of the state vector. The cost function I is defined as such,

$$I = \varpi_1 C_D + \varpi_2 \frac{1}{2} \sum_{NF} \left(p - p_T\right)^2 \Delta s, \quad (11)$$

where C_D is total wing drag coefficient, p is the current near field pressure, p_T is the target near field pressure, and ϖ_1 and ϖ_2 are weighting coefficients.

The variation of the cost function, δI, can be augmented by the discrete governing equations appropriately premultiplied by the adjoint variable $\psi^T_{i,j,k}$.

$$\delta I = \varpi_1 \delta C_D + \varpi_2 \sum_{NF} (p - p_T)\, \delta p \Delta s + \sum_{i=2}^{nx} \sum_{j=2}^{ny} \sum_{k=2}^{nz} \psi^T_{i,j,k} \delta \left(R(w) + D(w) \right)_{i,j,k}. \quad (12)$$

Here the first term represents the discrete drag minimization cost function, the second term represents the discrete remote inverse design cost function evaluated at a near field location which is approximately L chord length's away from the wing, $R(w)$ is the field equation, and $D(w)$ is the artificial dissipation term.

In order to eliminate δw from Eq (12), terms multiplied by the variation $\delta w_{i,j,k}$ of the discrete flow variables are collected and equated to zero. The following is the resulting discrete adjoint equation in a two dimensional domain,

$$\begin{aligned}
V\frac{\partial \psi_{i,j}}{\partial t} = & \\
& \left(\Delta y_{\eta_{i+\frac{1}{2},j}} \left[\frac{\partial f}{\partial w}\right]^T_{i,j} - \Delta x_{\eta_{i+\frac{1}{2},j}} \left[\frac{\partial g}{\partial w}\right]^T_{i,j} \right) \frac{\psi_{i+1,j}}{2} \\
& - \left(\Delta y_{\eta_{i-\frac{1}{2},j}} \left[\frac{\partial f}{\partial w}\right]^T_{i,j} - \Delta x_{\eta_{i-\frac{1}{2},j}} \left[\frac{\partial g}{\partial w}\right]^T_{i,j} \right) \frac{\psi_{i-1,j}}{2} \\
& + \left(\Delta x_{\xi_{i,j+\frac{1}{2}}} \left[\frac{\partial g}{\partial w}\right]^T_{i,j} - \Delta y_{\xi_{i,j+\frac{1}{2}}} \left[\frac{\partial f}{\partial w}\right]^T_{i,j} \right) \frac{\psi_{i,j+1}}{2} \\
& - \left(\Delta x_{\xi_{i,j-\frac{1}{2}}} \left[\frac{\partial g}{\partial w}\right]^T_{i,j} - \Delta y_{\xi_{i,j-\frac{1}{2}}} \left[\frac{\partial f}{\partial w}\right]^T_{i,j} \right) \frac{\psi_{i,j-1}}{2} \\
& - \left(\Delta y_{\eta_{i+\frac{1}{2},j}} \left[\frac{\partial f}{\partial w}\right]^T_{i,j} - \Delta x_{\eta_{i+\frac{1}{2},j}} \left[\frac{\partial g}{\partial w}\right]^T_{i,j} \right) \frac{\psi_{i,j}}{2} \\
& + \left(\Delta y_{\eta_{i-\frac{1}{2},j}} \left[\frac{\partial f}{\partial w}\right]^T_{i,j} - \Delta x_{\eta_{i-\frac{1}{2},j}} \left[\frac{\partial g}{\partial w}\right]^T_{i,j} \right) \frac{\psi_{i,j}}{2} \\
& - \left(\Delta x_{\xi_{i,j+\frac{1}{2}}} \left[\frac{\partial g}{\partial w}\right]^T_{i,j} - \Delta y_{\xi_{i,j+\frac{1}{2}}} \left[\frac{\partial f}{\partial w}\right]^T_{i,j} \right) \frac{\psi_{i,j}}{2} \\
& + \left(\Delta x_{\xi_{i,j-\frac{1}{2}}} \left[\frac{\partial g}{\partial w}\right]^T_{i,j} - \Delta y_{\xi_{i,j-\frac{1}{2}}} \left[\frac{\partial f}{\partial w}\right]^T_{i,j} \right) \frac{\psi_{i,j}}{2} \\
& + \delta d_{i+\frac{1}{2},j} - \delta d_{i-\frac{1}{2},j} + \delta d_{i,j+\frac{1}{2}} - \delta d_{i,j-\frac{1}{2}}.
\end{aligned} \quad (13)$$

Here V is the cell area and

$$\begin{aligned}
\delta d_{i+\frac{1}{2},j} \quad & = \epsilon^2_{i+\frac{1}{2},j} (\psi_{i+1,j} - \psi_{i,j}) - \epsilon^4_{i+\frac{3}{2},j} \psi_{i+2,j} \\
& + 3\epsilon^4_{i+\frac{1}{2},j} (\psi_{i+1,j} - \psi_{i,j}) + \epsilon^4_{i-\frac{3}{2},j} \psi_{i-1,j}
\end{aligned} \quad (14)$$

is the discrete adjoint artificial dissipation term which corresponds to the discretization of the inviscid flow equations by the Jameson-Schmidt-Turkel (JST) scheme. The dissipation coefficients ϵ^2 and ϵ^4 are functions of the flow variables, but, in order to reduce complexity, they are treated as constants. The effect of this partial discretization has been explored by Nadarajah et al.[18]

Discrete Adjoint Boundary Condition

This section illustrates the development of the discrete adjoint boundary condition for the calculation of remote sensitivities for supersonic flow. The $\delta w_{i,NF}$ term from the discrete cost function is added to the corresponding term from Eq (13). The discrete boundary condition appears as a source term in the adjoint fluxes. For example, at cell (i, NF) the adjoint equation can be discretized as follows,

$$\begin{aligned}
V\frac{\partial \psi_{i,NF}}{\partial t} = & -\frac{1}{2} A^T_{i-\frac{1}{2},NF} (\psi_{i,NF} - \psi_{i-1,NF}) \\
& - \frac{1}{2} A^T_{i+\frac{1}{2},NF} (\psi_{i+1,NF} - \psi_{i,NF}) \\
& - \frac{1}{2} B^T_{i,NF+\frac{1}{2}} (\psi_{i,NF+1} - \psi_{i,NF}) \\
& - \frac{1}{2} B^T_{i,NF-\frac{1}{2}} (\psi_{i,NF} - \psi_{i,NF-1}) + \Phi_{NF},
\end{aligned} \quad (15)$$

where V is the cell area, Φ_{NF} is the source term for inverse design,

$$\Phi_{NF} = -\varpi_1 (p - p_T) \Delta s_i \delta p_{i,NF},$$

and

$$A^T_{i+\frac{1}{2},NF} = \Delta y_{\eta_{i+\frac{1}{2},NF}} \left[\frac{\partial f}{\partial w}\right]^T_{i,NF} - \Delta x_{\eta_{i+\frac{1}{2},NF}} \left[\frac{\partial g}{\partial w}\right]^T_{i,NF}.$$

The wall boundary condition appears as source terms in the adjoint fluxes along the cells above the wall. The derivation of this boundary condition was explored by Nadarajah[18] et al. If a first order dissipation scheme is used, then Eq (14) would reduce to the term associated with ϵ^2. In such a case, the discrete adjoint equations are completely independent of the costate variables in the cells below the wall. However, if we use the blended first-and-third-order scheme, these flow variable values are required.

A simple zeroth-order extrapolation across the wall has produced good results, as shown by Nadarajah et al.[18]

Optimization Procedure

In this paper, the inverse design boundary condition is applied to the near field, while sensitivity derivatives or the gradient are calculated on the airfoil surface. The gradient for the discrete adjoint is obtained by perturbing each point on the lower wall. Once the gradient $\mathcal{G} = \frac{\partial I}{\partial b}$ has been determined, it can be used to drive a variety of gradient-based search procedures. The search procedure used in this work is a descent method in which small steps are taken in the negative gradient direction. Let $\mathcal{F}$ represent the design variable, and $\mathcal{G}$ the gradient. Then an improvement can be made with a shape change

$$\delta\mathcal{F} = -\lambda\mathcal{G}.$$

However, it is better to replace the gradient $\mathcal{G}$ by a smoothed value $\bar{\mathcal{G}}$ in the descent process. This acts as a preconditioner which allows the use of much larger steps and ensures that each new shape in the optimization sequence remains smooth. To apply smoothing in the ξ_1 direction, the smoothed gradient $\bar{\mathcal{G}}$ may be calculated from a discrete approximation to

$$\bar{\mathcal{G}} - \frac{\partial}{\partial\xi_1}\epsilon\frac{\partial\bar{\mathcal{G}}}{\partial\xi_1} = \mathcal{G}, \quad \bar{\mathcal{G}} = 0 \quad \text{at end points},$$

where ϵ is the smoothing parameter. If the modification is applied on the surface $\xi_2 =$ constant, then the first order change in the cost function is

$$\begin{aligned}
\delta I &= -\int\int \mathcal{G}\delta\mathcal{F}d\xi_1 \\
&= -\lambda\int\int\left(\overline{\mathcal{G}} - \frac{\partial}{\partial\xi_1}\epsilon\frac{\partial}{\partial\xi_1}\overline{\mathcal{G}}\right)\overline{\mathcal{G}}d\xi_1 \\
&= -\lambda\int\int\left(\overline{\mathcal{G}}^2 + \epsilon\left(\frac{\partial\overline{\mathcal{G}}}{\partial\xi_1}\right)^2\right)d\xi_1 \\
&< 0,
\end{aligned}$$

again guaranteeing an improvement unless $\bar{\mathcal{G}} = \mathcal{G} = 0$ and assuring an improvement if λ is sufficiently small and positive.

In some problems it turns out that the Hessian can be represented as a second order differential operator, so that with a proper choice of the smoothing parameter, the method becomes the Newton method. Search methods were intensively evaluated in a recent study by Jameson et al.,[28] and it was verified that these sample problems (which may have a high linear content) could be solved with a number of search steps independent of the number of design variables.

Implementation of Remote Inverse Design

The design procedure is as follows. First, the flow solver module is run until at least 5 orders of magnitude drop in the residual. Second, the cost function is calculated and the location of the source terms are determined. Third, the adjoint solver is run until at least 4 orders of magnitude drop in the residual. Next, the gradient is calculated by perturbing each point on the wing surface mesh. The resulting gradient is then smoothed by an implicit smoothing technique as described in the *Optimization Procedure* section. Then the wing geometry is updated and the grid is modified. The entire process is repeated until the conditions for optimality are satisfied. At each subsequent design iteration, 20 multigrid cycles for the flow and adjoint solver are used before the gradient is calculated. Figure (4) illustrates the design procedure.

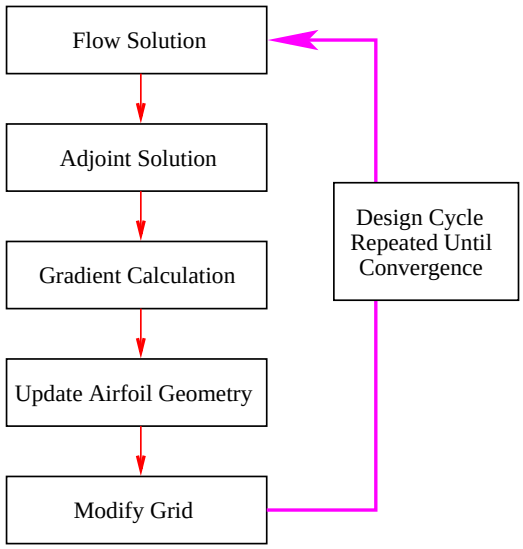

Figure 4: Design Procedure

Figure (5) shows the location of the near field pressure (+) and the adjoint remote sensitivity source terms (o). The variation of the cost function is first calculated by taking the difference between the current and target near field pressure at the (+)s for

every z-plane. A search algorithm then seeks for centers of cells that are within the cube defined by the (+) points. The search algorithm is repeated at every design cycle, since the possibility exists that the mesh may have modified and thus requiring a new location for the source term. The source terms are then computed using a trilinear interpolation at this location.

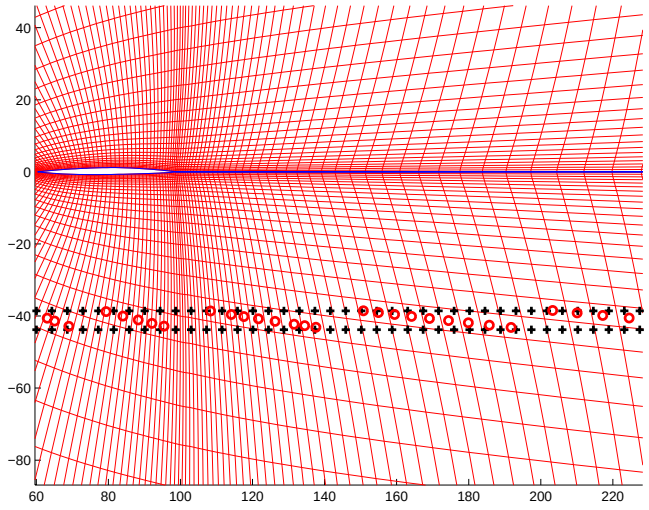

Figure 5: Location of Near Field Pressure and Adjoint Remote Sensitivity Source Terms

An alternative method for problems with more than one objective function, is to develop separate adjoint equations, one for each objective function. Both gradients are then calculated separately, multiplied by weights, and summed. A direction of improvement is then achieved with the new gradient. This method has the advantage that the user is better equipped with knowledge regarding the difference in magnitude between the two gradients. Appropriate weights can then be chosen to achieve the desired compromise. A disadvantage is the need to calculate a separate adjoint solution for each objective function.

In this work, we preferred to use a composite cost function, since we had apriori knowledge regarding the magnitude of the gradient contribution from the remote inverse cost function and the drag minimization cost function.

Results

This section presents the results of remote inverse and coupled remote inverse and drag minimization for three dimensional wings in supersonic flow. The objective is to reduce the peak pressure at the near field plane. Viscous effects are likely to be very small in these examples, so it is sufficient to use the Euler equations. The calculations were performed with a modified version of Jameson's SYN88 software, which augments the FLO88 flow solver with an adjoint solver, and shape modification procedures.

Biconvex Wing: Verification Study

To validate the use of our new method for the calculation of flow sensitivities, we have constructed the following test problem, based on a biconvex wing with a 3% thickness ratio at the root and 1.5% at the tip. The leading edge sweep of the wing is 7.125 degrees. The aspect ratio is 3.0 with a 0.218 taper ratio. To begin the remote inverse design process, the near field pressure distribution for a biconvex wing with a 2% thickness ratio at the root and 1% at the tip was first calculated in order to provide a realizable target pressure. All other wing geometry parameters were unchanged. The flow solution was obtained at a Mach Number of 1.5, at an angle of attack of 0 degrees, and the near field target pressure was computed at a distance of one chord length below the surface of the wing. Then we performed an inverse calculation with this target, starting from the 3% biconvex wing. Clearly, the solution of this problem is the reproduction of the 2% biconvex wing that initially produced the target pressure distribution.

Figures 6(a-b) illustrate the target (+), initial (□) , and final (∗) near field pressure distribution at the root and mid-span sections of the wing after 50 design cycles. An almost perfect point-to-point match is achieved. The objective function is the integral of the square of the difference between the current and target near field pressure. No lift or thickness constraints were enforced. These results clearly validate the remote adjoint method.

Biconvex Wing: Sonic Boom Reduction, Without Constraints

In order to illustrate the possibility of sonic boom reduction, a target pressure distribution was obtained by re-scaling the initial near field pressure distribution. Ultimately, this step will be replaced by a method that produces a target near field pressure

based upon the desired ground pressure signature. Here, in order to show a proof of concept of the remote inverse design method, re-scaled target pressures were chosen to produce a reduction in the near field peak pressure.

The target pressure was obtained using the FLO88 flow solver on a biconvex wing with a 5% thickness ratio at the root and 3.25% at the tip at a flight condition of $M = 1.5$ and a lift coefficient of $C_L = 0.1$ on a 192x32x32 C-grid. All other wing geometry parameters are the same as the previous section. The target pressure is then reduced by 40% of its original value.

Figures 7(a-b) illustrate the target (+), initial ($\square$), and final ($*$) near field pressure distribution. After 50 design cycles, the final near field pressure almost matches the target near field pressure. Neither the lift nor the thickness ratio at each span station were constrained.

Biconvex Wing: Sonic Boom Reduction, With Constraints

We now repeat the same design case but with the lift and thickness constrained. The value of the lift coefficient is maintained by adjusting the angle of attack to attain the desired lift coefficient. Thickness ratio at each span station is forced to remain the same.

The resulting solution is very different from the previous case. Figures 8(a-b) illustrates the baseline and optimized airfoil sections at span stations $z = 0.0957$ and $z = 0.571$.

Figures 9(a-b) show the target, initial, and final near field pressure distributions. The desired target pressure distribution is not achieved in contrast to the unconstrained case illustrated in Figure 7. In this case, there is a struggle between the near field peak pressure reduction versus maintenance of constant lift. Each design cycle, produces a shape modification that shifts the near field pressure distribution towards the target pressure. Unfortunately, this also causes a reduction in the lift coefficient. This must be compensated by an increase in the angle of attack to maintain the total lift coefficient, which in turn leads to an increase in the near field peak pressure. After 50 design cycles, the solution converges to the $(- * -)$ line in Figure 9. The final peak pressure has been reduced to almost 23% its original value at the root section and 18% at the mid-span section.

Design Case	C_D	$C_D(\%)$
Baseline	0.00382	
Remote Inverse	0.00395	+3.4%
Drag Minimization	0.00320	−16.2%
Remote Inverse and Drag Min.	0.00360	−5.8%

Table 1: Total Wing Drag Coefficient for Various Design Cases

Highly Swept Blunt LE Wing: Sonic Boom and Drag Reduction

The previous examples are wings with low sweep back and sharp supersonic leading edges. Here we examine a highly swept wing with a blunt subsonic leading edge. Blunt leading edge symmetric airfoils were created with a thickness ratio of 4% at each span station. The wing has 60 degrees leading edge sweep, and a 0.5624 taper ratio.

Figures 10(a-b) illustrate the airfoil sections at span locations $z = 0.0957$ and $z = 0.571$. Each figure contains three plots: Baseline Wing, Wing Optimized with Remote Inverse Objective Function, and Wing Optimized with Remote Inverse and Drag Minimization Objective Functions. The airfoil sections are scaled to exaggerate the modifications. Figures 11(a-b) show the corresponding near field pressure distribution at the same span locations. At the root section, a 14.2% reduction in the peak pressure was obtained with the remote inverse as the objective function and a slightly smaller reduction of 13.0% was achieved with the weighted sum of the remote inverse and drag minimization cost functions. At the mid span location, a 10.4% reduction was achieved with the former and 9.4% reduction with the latter cost function. For the case of joint drag minimization and remote inverse design, the weights were $\varpi_1 = 0.005$ and $\varpi_2 = 1.0$. The weighting coefficient for the drag minimization cost function had to be considerably smaller due to the larger magnitude of its gradient contribution. Since the main objective of the design is to reduce the near field peak pressure, the weights were adjusted to achieve the desired result. A comparison of the two final designs achieved by the remote inverse and the joint remote inverse and drag minimization cost functions show that the two methods provide similar results, with the remote inverse cost function providing a very slightly greater reduction in the near field pressure peak.

Table 1 lists the total wing drag coefficient for the baseline wing and the optimized wings. If only the

remote inverse cost function was used, then a 3.4% increase in total drag is seen versus the 5.8% reduction in total drag with the dual objective function case. The reason for the difference between the two final designs can be seen clearly in Figures 12(a-d). Figure 12(a) illustrates the pressure contour of the upper surface of the wing. A strong shock is present slightly aft of the mid chord location at the wing tip. The shock strength weakens as it moves inboard. Figure 12(b) shows the pressure contour of the final design using only the remote inverse cost function. Here we notice the presence of the shock wave at the wing tip. In Figure 12(c) this shock is eliminated in the design case using only the drag minimization objective function. However, in Figure 12(d) it is clearly seen that the wing tip shock strength is reduced, thus contributing to the reduction in the total drag coefficient.

Figures 13(a-c) illustrate the coefficient of pressure plots for the baseline and the two redesigned wings at three different span locations. At $z = 0.85$, the plots clearly show the reduction in the strength of the shock.

Conclusions

The results demonstrate the feasibility of remote inverse calculations using the adjoint method, which would be impossible with other inverse methods such as CDISC[29] . An application to the sonic boom minimization resulted in an 18% reduction in the near field peak pressure for the low swept biconvex wing and 10% for the highly swept blunt leading edge wing. It proved highly beneficial to use a composite cost function consisting of the sum of the weighted remote inverse and drag minimization cost functions, resulting in final wing designs that produced both lower near field peak pressures and lower total wing drag coefficients.

Acknowledgments

This research has benefitted greatly from the generous support of the AFOSR under grant number AF F49620-98-1-022

References

[1] R. Seebass, B. Argrow. *Sonic Boom Minimization Revisited. AIAA paper 98-2956*, AIAA 2nd Theoretical Fluid Mechanics Meeting, Albuquerque, NM, June 1998.

[2] F. Bauer, P. Garabedian, D. Korn, and A. Jameson. *Supercritical Wing Sections II.* Springer-Verlag, New York, 1975

[3] P. Garabedian, and D. Korn. Numerical Design of Transonic Airfoils *Proceedings of SYNSPADE 1970.* pp 253-271, Academic Press, New York, 1971.

[4] R. M. Hicks and P. A. Henne. Wing Design by Numerical Optimization. *Journal of Aircraft.* 15:407-412, 1978.

[5] J.L. Lions. *Optimal Control of Systems Governed by Partial Differential Equations.* Springer-Verlag, New York, 1971. Translated by S.K. Mitter.

[6] O. Pironneau. *Optimal Shape Design for Elliptic Systems.* Springer-Verlag, New York, 1984.

[7] A. Jameson. Aerodynamic design via control theory. In *Journal of Scientific Computing*, 3:233-260,1988.

[8] A. Jameson. Automatic design of transonic airfoils to reduce the shock induced pressure drag. In *Proceedings of the 31st Israel Annual Conference on Aviation and Aeronautics, Tel Aviv*, pages 5–17, February 1990.

[9] A. Jameson. Optimum aerodynamic design using CFD and control theory. *AIAA paper 95-1729*, AIAA 12th Computational Fluid Dynamics Conference, San Diego, CA, June 1995.

[10] A. Jameson, N. Pierce, and L. Martinelli. Optimum aerodynamic design using the Navier-Stokes equations. In *AIAA 97-0101*, 35th. Aerospace Sciences Meeting and Exhibit, Reno, Nevada, January 1997.

[11] A. Jameson., L. Martinelli, and N. Pierce. Optimum aerodynamic design using the Navier-Stokes equations. In *Theoretical Computational Fluid Dynamics*, 10:213-237, 1998.

[12] A. Jameson, J. Alonso, J. Reuther, L. Martinelli, J. Vassberg. Aerodynamic Shape Optimization Techniques Based on Control Theory. In *AIAA 98-2538*, 29th. AIAA Fluid Dynamics Conference, Alburquerque, NM, June 15-18 1998.

[13] A. Jameson, L. Martinelli, J. Alonso, J. Vassberg, J. Reuther. Perspective on Simulation Based Aerodynamic Design. Computational

Fluid Dynamics for the 21st. Century. In *Proceedings of a Symposium Honoring Prof. Satofuka on the Occasion of his 60th. Birthday, Kyoto, Japan.* 15-17 July, 2000

[14] J. Vassberg and A. Jameson. Aerodynamic Shape Optimization of a Reno Race Plane. In *International Journal of Vehicle Design*, 28:No.4:318-338, 2002.

[15] J. Reuther and A. Jameson. Aerodynamic shape optimization of wing and wing-body configurations using control theory. *AIAA 95-0213*, 33rd Aerospace Sciences Meeting and Exibit, Reno, Nevada, January 1995.

[16] J. Reuther, A. Jameson, J. J. Alonso, M. J Rimlinger, and D. Saunders. Constrained multipoint aerodynamic shape optimization using an adjoint formulation and parallel computers. *AIAA 97-0103*, AIAA 35th Aerospace Sciences Meeting and Exhibit, Reno, NV, January 1997.

[17] G. W. Burgreen and O. Baysal. Three-Dimensional Aerodynamic Shape Optimization of Wings Using Discrete Sensitivity Analysis. *AIAA Journal*, Vol. 34, No.9, September 1996, pp. 1761-1770.

[18] S. Nadarajah and A. Jameson. A Comparison of the Continuous and Discrete Adjoint Approach to Automatic Aerodynamic Optimization. *AIAA 00-0667*, AIAA 38th. Aerospace Sciences Meeting and Exhibit, Reno, NV, January 2000.

[19] S. Nadarajah and A. Jameson. Studies of the Continuous and Discrete Adjoint Approaches to Viscous Automatic Aerodynamic Shape Optimization *AIAA 2001-2530*, AIAA 15th. Computational Fluid Dynamic Conference, Anaheim, Ca, June 11-14, 2001.

[20] J. Alonso, A. Jameson, and I. Kroo. Advanced Algorithms for Design and Optimization of Quiet Supersonic Platforms. *AIAA 2002-0144*, AIAA 40th. Aerospace Sciences Meeting and Exhibit, Reno, NV, January 2002.

[21] S. Nadarajah, A. Jameson, J. Alonso. An Adjoint Method for the Calculation of Non-Collocated Sensitivities in Supersonic Flow. In *Proceedings of First MIT Conference on Computational Fluid and Solid Mechanics*, June 12-15, 2001.

AIAA 2001-2530, AIAA 15th. Computational Fluid Dynamic Conference, Anaheim, Ca, June 11-14, 2001.

[22] G. R. Shubin and P. D. Frank. A Comparison of the Implicit Gradient Approach and the Variational Approach to Aerodynamic Design Optimization. *Boeing Computer Services Report AMS-TR-163*, April 1991.

[23] F. Beux and A. Dervieux. Exact-Gradient Shape Optimization of a 2-D Euler Flow. *Finite Elements in Analysis and Design*, Vol. 12, 1992, 281-302.

[24] J. Elliot and J. Peraire. Aerodynamic Design Using Unstructured Meshes. *AIAA 96-1941*, 1996.

[25] W. K. Anderson and V. Venkatakrishnan. Aerodynamic Design Optimization on Unstructured Grids with a Continuous Adjoint Formulation. *AIAA 96-1941*, 1996.

[26] A. Iollo, M. Salas, and S. Ta'asan. Shape Optimization Gorvened by the Euler Equations Using and Adjoint Method. *ICASE report 93-78*, November 1993.

[27] S. Ta'asan, G. Kuruvila, and M. D. Salas. Aerodynamic design and optimization in one shot. *AIAA 91-0025*, 30th Aerospace Sciences Meeting and Exibit, Reno, Nevada, January 1992.

[28] A. Jameson and J. Vassberg. Studies of Alternative Numerical Optimization Methods Applied to the Brachistochrone Problem.

[29] R. Campbell. and Smith. L. A Hybrid Algorithm for Transonic Airfoil and Wing Design. *AIAA 87-2552-CP*,1987.

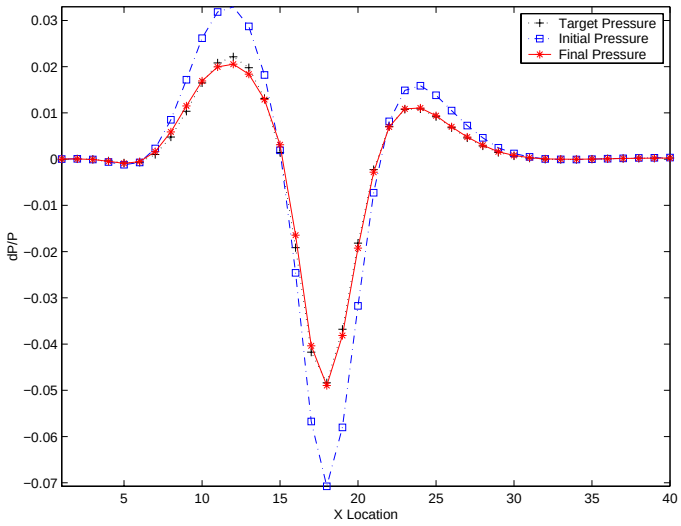

6a: z = 0.0957

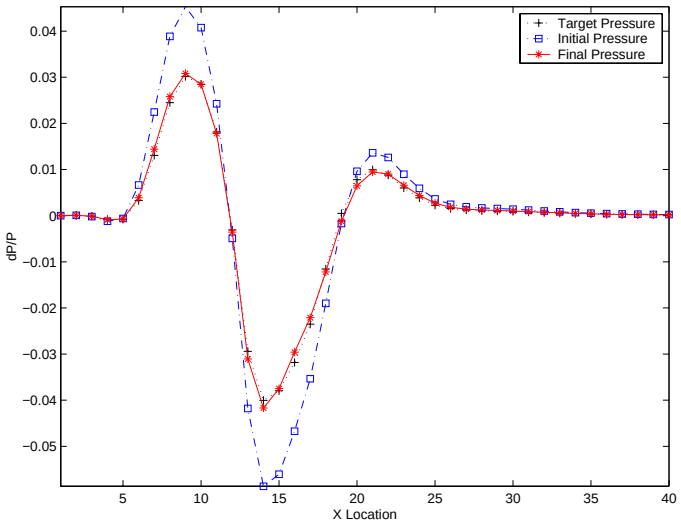

6b: z = 0.571

Figure 6: Verification Study: Target, Initial, and Final Near Field Pressure Distribution Mach = 1.5, $\alpha = 0$ deg.

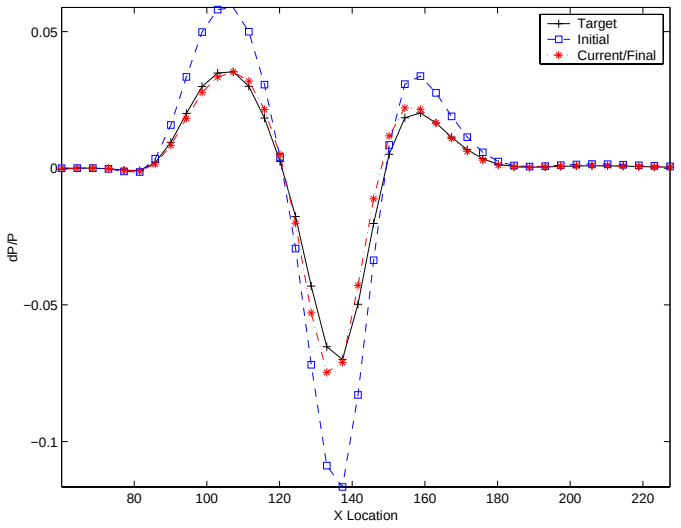

7a: z = 0.0957

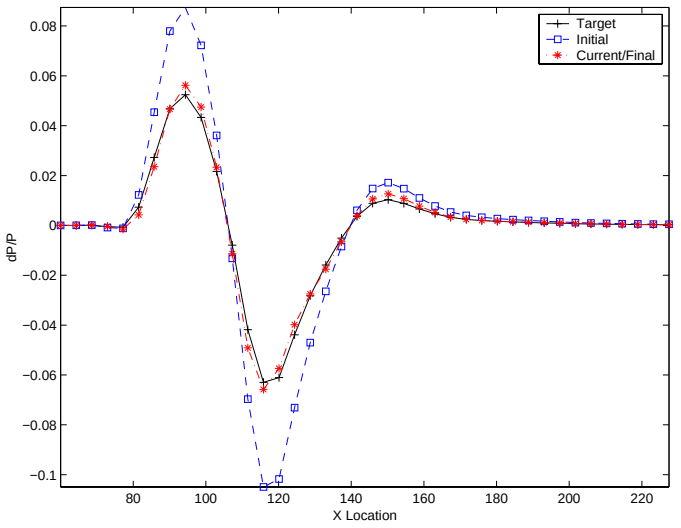

7b: z = 0.571

Figure 7: Sonic Boom Minimization: Target, Initial, and Final Near Field Pressure Distribution after 50 Design Cycles. Mach = 1.5, $\alpha = 1.75$ deg., No Lift Coefficient and Thickness Ratio Constraints

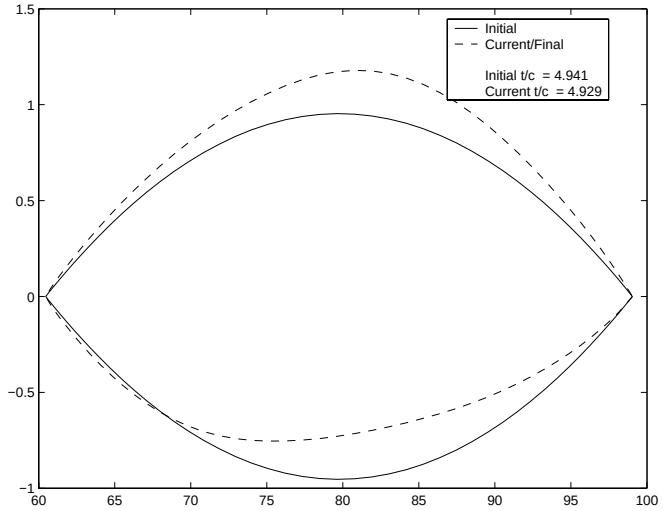

8a: z = 0.0957

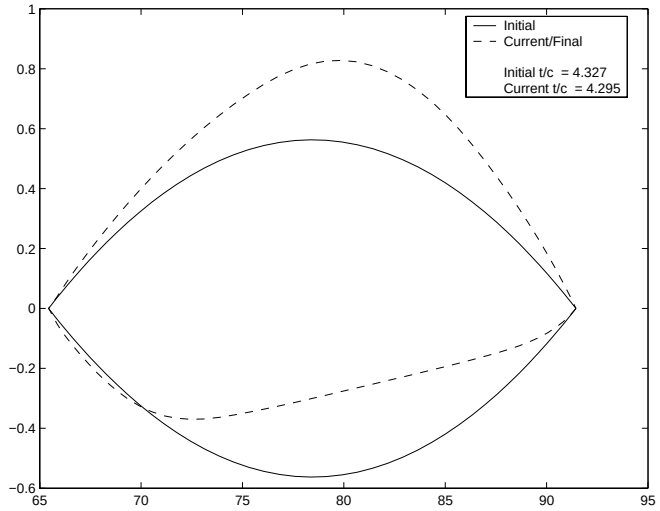

8b: z = 0.571

Figure 8: Sonic Boom Minimization: Initial and Final Airfoil Shape After 50 Design Cycles
Mach = 1.5, $\alpha = 1.75$ deg, Fixed Lift Coefficient = 0.1, Fixed Thickness Ratio

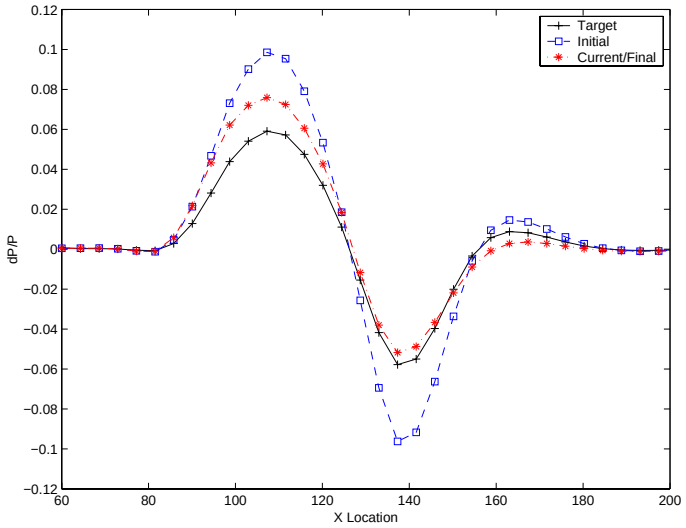

9a: z = 0.0957

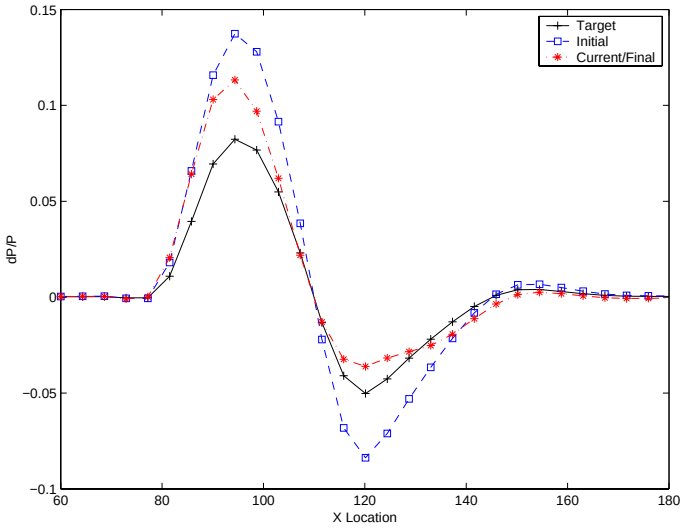

9b: z = 0.571

Figure 9: Sonic Boom Minimization: Target, Initial, and Final Near Field Pressure Distribution after 50 Design Cycles. Mach = 1.5, $\alpha = 1.75$ deg., Fixed Lift Coefficient = 0.1, Fixed Thickness Ratio

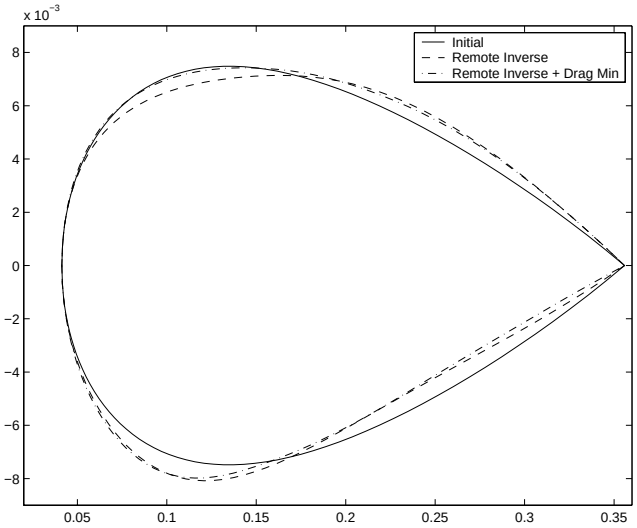

10a: z = 0.0957

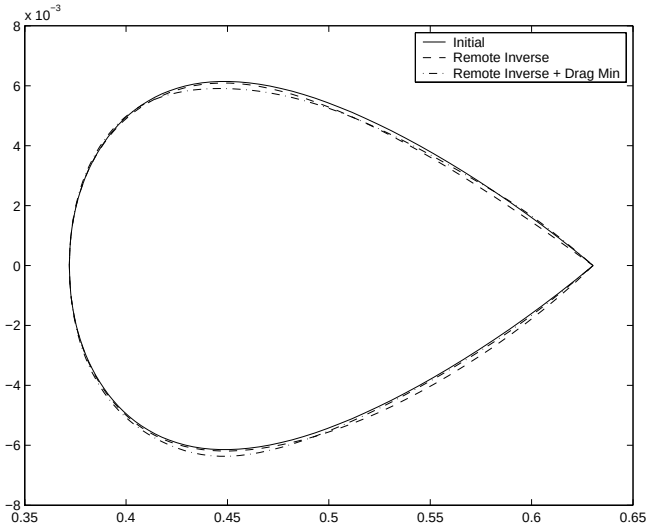

10b: z = 0.571

Figure 10: Sonic Boom and Drag Minimization: Initial and Final Airfoil Shape After 50 Design Cycles Mach = 1.5, $\alpha = 0.829$ deg, Fixed Lift Coefficient = 0.05, Fixed Thickness Ratio

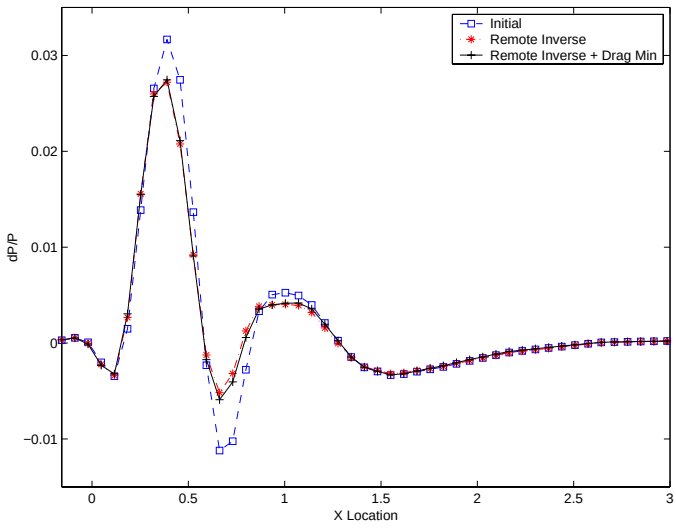

11a: z = 0.0957

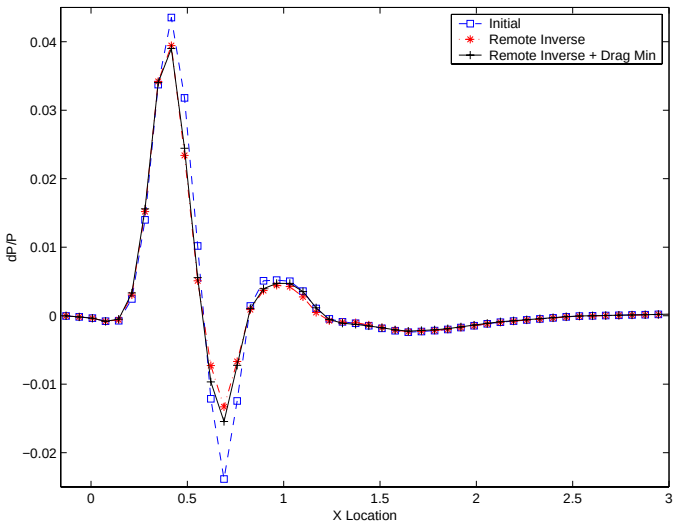

11b: z = 0.571

Figure 11: Sonic Boom and Drag Minimization: Target, Initial, and Final Near Field Pressure Distribution after 50 Design Cycles. Mach = 1.5, $\alpha = 0.829$ deg., Fixed Lift Coefficient = 0.05, Fixed Thickness Ratio

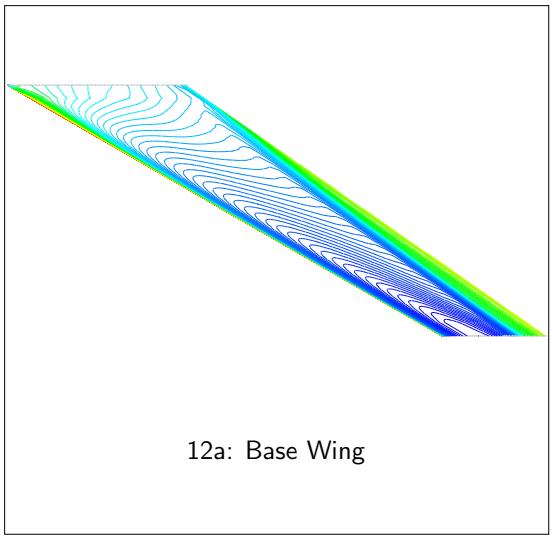

12a: Base Wing

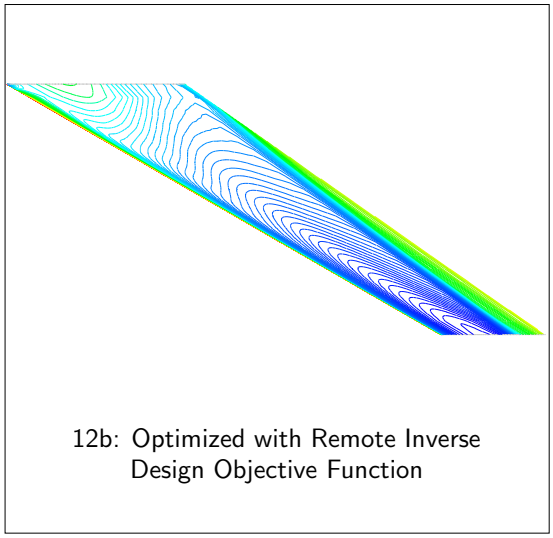

12b: Optimized with Remote Inverse Design Objective Function

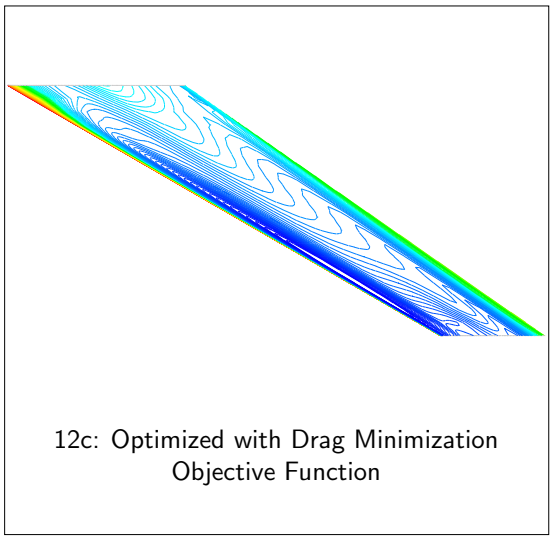

12c: Optimized with Drag Minimization Objective Function

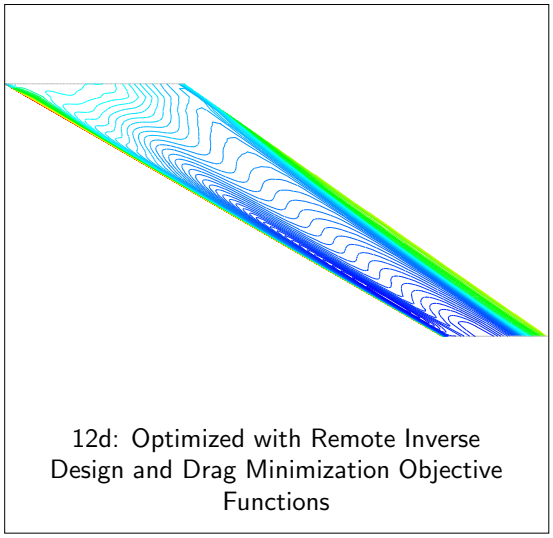

12d: Optimized with Remote Inverse Design and Drag Minimization Objective Functions

Figure 12: Sonic Boom and Drag Minimization: Pressure Contours of Final Design of the Upper Surface of the Wing. Mach = 1.5, $\alpha = 0.829$ deg, Fixed Lift Coefficient = 0.05, Fixed Thickness Ratio

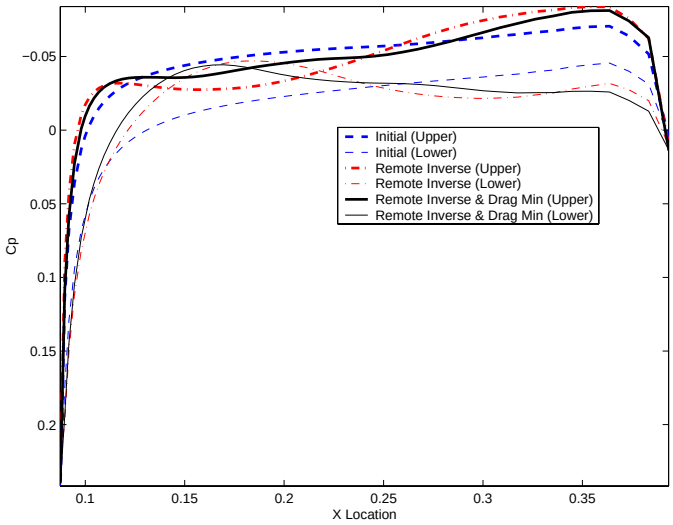

13a: z = 0.0957

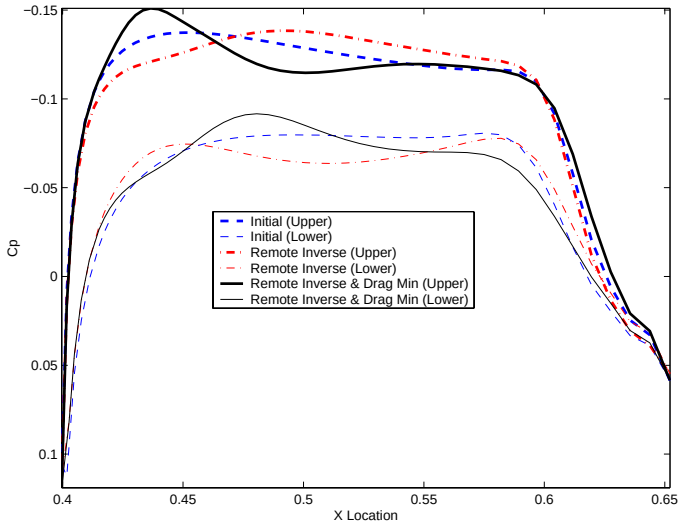

13b: z = 0.5

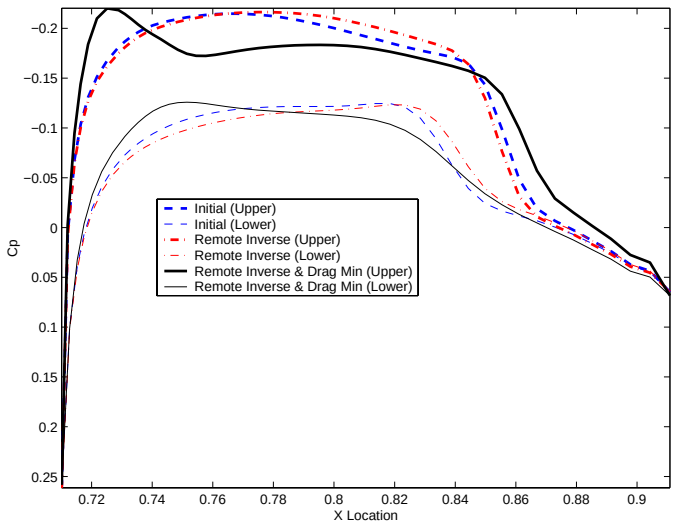

13c: z = 0.85

Figure 13: Sonic Boom and Drag Minimization: Surface Pressure Coefficient. Mach = 1.5, $\alpha = 0.829$ deg, Fixed Lift Coefficient = 0.05, Fixed Thickness Ratio